http://dx.doi.org/10.5012/bkcs.2013.34.3.899

Docking, CoMFA and CoMSIA Studies of a Series of *N*-Benzoylated Phenoxazines and Phenothiazines Derivatives as Antiproliferative Agents

Jahan B. Ghasemi,* Elham Aghaee, and Ali Jabbari

Chemistry Department, Faculty of Sciences, K. N. Toosi University of Technology, Tehran, Iran
**E-mail: Jahan.ghasemi@gmail.com*
Received October 15, 2012, Accepted December 26, 2012

Using generated conformations from docking analysis by Gold algorithm, some 3D-QSAR models; CoMFA and CoMSIA have been created on 39 *N*-benzoylated phenoxazines and phenothiazines, including their *S*-oxidized analogues. These molecules inhibit the polymerization of tubulin into microtubules and thus they have been studied for the development of antitumor drugs. Training set for the CoMFA and CoMSIA models using 30 docked conformations gives q^2 Leave one out (LOO) values of 0.756 and 0.617, and r^2 ncv values of 0.988 and 0.956, respectively. The ability of prediction and robustness of the models were evaluated by test set, cross validation (leave-one-out and leave-ten-out), bootstrapping, and progressive scrambling approaches. The all-orientation search (AOS) was used to achieve the best orientation to minimize the effect of initial orientation of the structures. The docking results confirmed CoMFA and CoMSIA contour maps. The docking and 3D-QSAR studies were thoroughly interpreted and discussed and confirmed the experimental pIC_{50} values.

Key Words : Phenoxazines and phenothiazines derivatives, Tubulin, CoMFA, CoMSIA, Docking

Introduction

Microtubules are long, hollow cylindrical biopolymers that are composed of subunits made from a globular cytoplasmic protein known as tubulin, as illustrated in Figure 1. Each subunit of the microtubule is made of two slightly different but closely related simpler units called α-tubulin and β-tubulin that are bound very tightly together to form heterodimers. These rope-like polymers of tubulin play an important role in the migration of chromosomes to opposite ends of a mitosing cell during the anaphase. Microtubules are one of the most successful cancer chemotherapeutic targets since they are responsible for mitotic spindle formation and proper chromosomal separation.[1-4] Various drugs have been shown to bind specifically to tubulin in the mitotic spindle and prevent polymerization into the microtubules. Thus these drugs inhibit cell mitosis and lead to cell death.[5-7] Colchicine is one of the most effective inhibitors of tubulin polymerization,[8] however, because of its narrow therapeutic window, colchicine has not found broad application in anticancer therapy. Therefore, there is an urgent need to design and develop new antimitotic agents. The promising usage of microtubule-binding drugs for anticancer therapy created great interest in designing microtubule-targeted drugs so great efforts have recently been made to design novel small-molecular tubulin binders.[9-11]

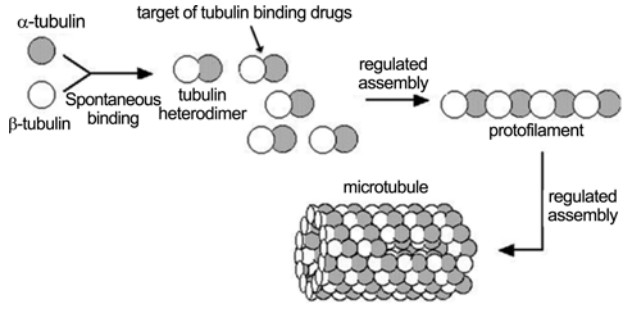

Figure 1. Structure of microtubule as a target of various anticancer drugs.

Quantitative structure-activity relationship (QSAR) studies perform a vital role in drug discovery and drug design as ligand-based approaches. One would say that today no drug is developed without previous QSAR analyses.

The primary aim of QSAR methods is to correlate structural descriptors with biological properties, but it can also be applied to predict the activity value of non-synthesized compounds structurally related to the training sets and helps to clarify the possible molecular mechanism of the receptor-ligand interactions.[12-16]

Three-dimensional quantitative structure-activity relationship (3D-QSAR) analysis is a common method used in computer-assisted molecular design. Among the 3D-QSAR methods, the comparative molecular field analysis (CoMFA), proposed by Cramer and co-workers, is extensively used in the current practice of drug discovery which it provides the visual display of electrostatic (Coulomb) and steric (Lennard-Jones) fields of the regions important for biological activity.[17] In a similar method, comparative molecular similarity indices analysis (CoMSIA), a probe atom is used to calculate similarity indices, at regularly spaced grid points for the aligned molecules. CoMSIA differs from CoMFA, initially in the way that the molecular fields are calculated, which uses a Gaussian-type distance-dependent function to assess five fields of different physicochemical properties (*i.e.*, steric, electrostatic, hydrophobic, and hydrogen bonding donor and acceptor).[18,19] In computational drug design, molecular dock-

ing is applied to gain key structural features of binding of molecules into the receptor and predicting bioactive conformers.[20-23] In recent years, a number of QSAR and docking studies have been carried out for predicting new tubulin polymerization inhibitors as anticancer drugs.[24-26]

In this study, 3D-QSAR approaches based on docking alignments were applied to construct predictive 3D-QSAR models on a new class of *N*-benzoylated phenoxazines and phenothiazines which applied to design new and more potent antitumor drugs.

Experimental

Data Set. A collection of 39 compounds was reported

Table 1. Structures and activities of *N*-benzoylated phenoxazines and phenothiazines derivatives

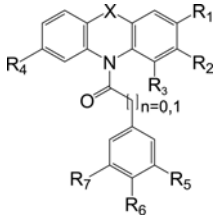

Comp.	n	x	R_1	R_2	R_3	R_4	R_5	R_6	R_7	pIC_{50}
1	0	O	H	H	H	H	H	OCH_3	H	7.4815
2[a]	1	O	H	H	H	H	H	OCH_3	H	5.3178
3	0	O	H	Cl	H	H	H	OCH_3	H	6.8539
4	0	O	H	Cl	H	H	OCH_3	H	H	5.8601
5	1	O	H	Cl	H	H	H	OCH_3	H	6.2596
6	0	O	H	Cl	H	H	OH	OCH_3	H	7.0969
7	0	O	H	Cl	H	H	OCH_3	OH	OCH_3	5.3344
8	0	O	H	Cl	H	H	OCH_2O	OCH_2O	H	5.9508
9[a]	0	O	H	Cl	H	H	OCH_3	OCH_3	OCH_3	4.6198
10	0	O	H	Cl	H	H	H	Cl	H	4.6989
11	0	O	H	Cl	H	H	H	$N(CH_3)_2$	H	5.9172
12	0	O	H	Cl	H	Cl	H	OCH_3	H	6.3098
13[a]	0	O	H	CN	H	H	H	OCH_3	H	6.7959
14	0	O	CN	H	H	H	H	H	H	6.6383
15[a]	0	O	CN	H	H	H	H	OCH_3	H	7.8539
16	0	O	CN	H	H	H	OH	OCH_3	H	7.9586
17	0	O	CN	H	H	H	H	Cl	H	6.3098
18	0	O	H	H	CN	H	H	OCH_3	H	6.9208
19[a]	0	S	H	H	H	H	H	OCH_3	H	6.4815
20	0	S	H	H	H	H	OCH_3	OCH_3	OCH_3	5.7305
21	0	S	H	H	H	H	OH	OCH_3	H	6.6778
22	0	S	H	Cl	H	H	H	OCH_3	H	6.0757
23	0	S	H	Cl	H	H	OCH_3	OCH_3	OCH_3	4.9586
24	1	S	H	Cl	H	H	H	OCH_3	H	5.0969
25	0	S	H	CF_3	H	H	H	OCH_3	H	5.3372
26[a]	0	S	H	OCH_3	H	H	H	OCH_3	H	6.0132
27	0	S	H	SCH_3	H	H	H	OCH_3	H	5.4413
28	0	SO	H	H	H	H	H	OCH_3	H	6.3767
29	0	SO	H	H	H	H	OCH_3	OCH_3	OCH_3	5.0953
30	0	SO	H	H	H	H	OH	OCH_3	H	6.5229
31[a]	0	SO	H	Cl	H	H	H	OCH_3	H	5.8539
32	0	SO	H	Cl	H	H	OCH_3	OCH_3	OCH_3	4.4559
33	0	SO	H	OCH_3	H	H	H	OCH_3	H	5.7825
34	0	SO_2	H	H	H	H	H	OCH_3	H	6.5528
35[a]	0	SO_2	H	H	H	H	OCH_3	OCH_3	OCH_3	5.5850
36	0	SO_2	H	H	H	H	OH	OCH_3	H	6.7447
37	0	SO_2	H	Cl	H	H	H	OCH_3	H	6.0969
38	0	SO_2	H	Cl	H	H	OCH_3	OCH_3	OCH_3	5.3767
39	0	SO_2	H	OCH_3	H	H	H	OCH_3	H	5.8013

[a]Prediction set

recently by H. Prinz and co-workers,[27] as a new class of antiproliferative agents, was used for docking and 3D-QSAR analysis. The activity (IC_{50}) values of some molecules had been reported qualitative (*i.e.* they have not exact quantities for activities), so these molecules were removed from the data set. For the QSAR analysis the IC_{50} (μM) values were taken in molar range and were expressed in negative logarithmic units, pIC_{50} ($-logIC_{50}$). The chemical structures and corresponding pIC_{50} are listed in Table 1. The set of compounds was divided into training and test sets. The test set compounds were selected by considering both the distribution of biological data and structural diversity of the molecules. The compound no. 5 shows large residual value, so identified as outliers and removed from the training set, and the compound no. 16 was used as a template because of the highest activity.

Molecular Docking. The crystal structure of tubulin (1SA0) was taken from RCSB protein databank (http://www.pdb.org). This protein in PDB is not complexed with anyone of the understudy ligands, so in docking step its original ligand (colchicine) was removed and then ligands in our data set were docked in the active site of tubulin one by one. Ligands preparation step was carried out in SYBYL 7.3 molecular modeling package (Tripos Inc., St. Louis, USA) running on a Red Hat Linux workstation 4.7. The resulting structures were imported into Discovery Studio 2.5 (Accelrys Inc, San Diego, CA, USA), and typed with CHARMm force field then partial charges were calculated by Momany-Rone option.[28] Then they were minimized with Smart Minimizer which performs 1000 steps of steepest descent with a RMS gradient tolerance of 3, followed by conjugate gradient minimization. For preparation step of tubulin, all complexes were typed with CHARMm force field, hydrogen atoms were added, all water molecules were removed and pH of protein was adjusted to almost neutral, 7.4, using protein preparation protocol. All of antitumor molecules were again minimized *in-situ* with Smart Minimizer option that is custom for *in-situ* ligand minimization and consists of some pre-defined minimization steps that have been pre-determined to work well for receptor ligand data.[29] The protein active site was defined as a sphere with a radius of 10 Å around the bounded ligand to confirm atoms of the ligand and the side-chains of the residues of the receptor within 10 Å from the center of the binding site are free to move. Then bounded ligand was removed from the binding site. Other parameters were set by default protocol settings. GOLD program was used to dock inhibitors into receptor.[30] It is complicated to predict how a small molecule will bind to a protein, and no method can guarantee success. However, GOLD has a correct solution in 70-80% of cases.[31]

CoMFA and CoMSIA. Molecular modeling studies were performed using the SYBYL 7.3 molecular modeling package (Tripose Inc., St. Louis, USA) running on a Red Hat Linux workstation 4.7. Molecular structures were built using the SKETCH option in SYBYL. Energy minimization was performed using the Tripos force field with a distance dependent dielectric and the Powell conjugate gradient algorithm with a convergence criterion of 0.01 kcal/mol Å. Partial atomic charges were calculated using the Gasteiger-Hückel method.

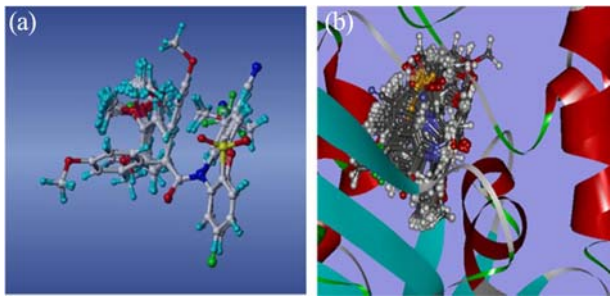

Figure 2. Alignment of compounds based on (a) rigid body alignment based on compound **16** and (b) docking alignment inside the active site.

Two methods were used to generate 3D-QSAR models. In first approach the compounds were aligned to template molecule (compound **16**) on a backbone which is common among all structures to minimize the sum-of-squares deviation between reference backbone in each molecule and the corresponding core in the template (Figure 2(a)). In CoMFA a sp3 carbon atom with +1 charge was used as a probe to calculate steric and electrostatic interactions between the probe and structures. Coulomb and Lennard-Jones potentials were used to model Electrostatic and van der Waals interactions, respectively. Energy cut off values of 30 kcal/mol was selected for both steric and electrostatic fields. Various column filtering values are also tested. Threshold column filtering of 2.0 kcal/mol was set to accelerate the analysis and reduce the amount of noise. CoMFA standard scaling applies the equal weight to data from each lattice point in any given field. Region focusing is an iterative procedure which refines a model by improving the weight for those lattice points which are most related to the model. This upgrades the resolution and predictive capability (q^2; cross validated r^2) of a followed PLS analysis. Technically, this corresponds to rotate the model components during a high-order space.[32] PLS region focusing is rationally equivalent to the GOLPE strategy and q^2-GRS.[33,34] In CoMSIA, standard settings (probe with charge +1, radius 1Å and hydrophobicity +1, hydrogen-bond donating +1, hydrogen-bond accepting +1, grid spacing 2 Å) were used to calculate five different fields: steric, electrostatic, hydrophobic, hydrogen bond acceptor and donor. In 3D-QSAR, PLS analysis was used for modeling in which the independent variables were the CoMFA and CoMSIA fields, and pIC_{50} activity values were used as dependent variables. The predictive ability of the models was evaluated by leave one out (LOO) cross-validation. LOO cross-validation method was used to obtain the optimal number of components (latent variables) in the subsequent analysis. Analysis of CoMFA and CoMSIA results and the prediction of the models were performed by non-cross validation method according to SYBYL terminology. The progressive scrambling method was carried out for the evaluation of the sensitivity of the 3D-QSAR model to

chance correlations. As a final method of validation of the derived models, pIC_{50} of 8 compounds, as external test set, were predicted using models derived from the training set.

Different space orientations of the molecular collective in the grid box have important effect on 3D-QSAR models, so all-orientation search (AOS) was also performed on initial orientations of aligned structures by the rotation procedure written in SYBYL programming language (SPL).[35]

In the second strategy all molecules were minimized inside the active site of tubulin and then docked by GOLD software, then the best pose of each molecule was selected and docked conformers were fed to SYBYL molecular modeling package (Figure 2(b)) and other steps were performed like first strategy.

Results and Discussion

Docking Results. Docking computations were employed to find the probable binding conformations of all molecules. To validate the docking reliability, root-mean-square distance (RMSD) value was calculated between bounded ligand and redocked ligand (colchicine), which was 1.26 Å in this method. This value shows that there is high reliability of GOLD method to reproduce the known binding mode of these inhibitors. Detailed analysis of the binding mode of the best docked pose of molecule 16 shows a hydrogen bond between C=O substituent and Val181 from the α chain and another hydrogen bond between CN group and Cys241 from the β chain of tubulin, same as it can be seen by hydrogen bond acceptor feature near the CN group, enhancing its binding in the pocket of tubulin and that's why compounds **15** and **16** are the most active compounds in the set (Figure 3).

According to docking results, there is an interaction between these antitubulin molecules and three residues of β chain of tubulin (Lys254, Ala250 and Leu248) and Asn101 from α chain, by the terminal OCH_3 (R6). On the other hand, the OH group in R5 position has interactions with NH group of Leu255 and the C=O group of Lys254 from β chain and two hydrogens of Asn101 from α chain. R_2 is in Van der Waals contact with the hydrophobic parts of Leu248 (β chain), and R_7 is in Van der Waals contact with the hydrophobic parts of Ala180 (α chain) and Lys 254 (β chain). Because of probable steric clashes with boundaries of the pocket, more bulky groups such as OCH_3 would decrease the activity. There are electrostatic interaction between the x substituent and Leu255, Met259, Ala316 and Lys352 from β chain. Figure 4 shows the MOLCAD surfaces structure representing electrostatic and lipophilic potential of the tubulin pocket by the use of compound **16**. The electrostatic potential color ramp ranges from blue (most electronegative potential values) to red (most electropositive potential values) and the lipophilic potential color ramp ranges from blue (low lipophilic potential values) to brown (high lipophilic potential values).

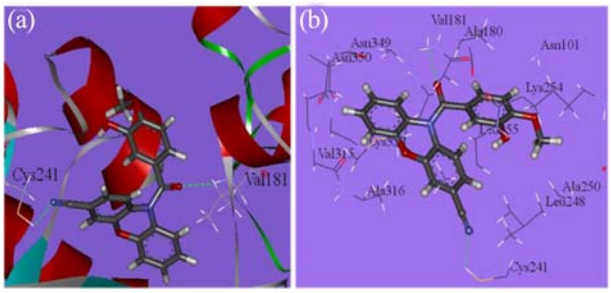

Figure 3. The best docked conformation of the most active compound (compound **16**) in the binding site of tubulin results two hydrogen bonds (a) protein is shown in secondary type (b), the close residues of tubulin are shown.

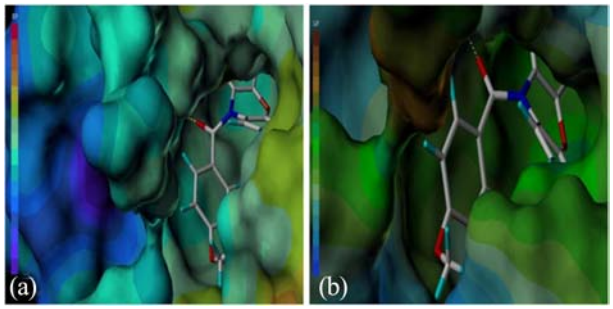

Figure 4. The MOLCAD surfaces structure depicted with (a) electrostatic and (b) lipophilic potential of the tubulin pocket using compound **16**. The electrostatic potential color ramp ranges from blue (most electronegative potential values) to red (most electropositive potential values) and the lipophilic potential color ramp ranges from blue (low lipophilic potential values) to brown (high lipophilic potential values).

Table 2. Summary of the statistical results for the constructed models

Statistical Parameters[a]	Rigid alignment			Docking alignment		
	CoMFA (CF = 2.9)	CoMFA-RF (CF = 2.9)	CoMSIA (CF = 2.6)	CoMFA (CF = 2.3)	CoMFA-RF (CF = 2.0)	CoMSIA (CF = 2.0)
q^2	0.482	0.611	0.617	0.645	0.756	0.673
SEP	0.640	0.564	0.642	0.551	0.457	0.507
r^2 ncv	0.871	0.910	0.899	0.989	0.988	0.956
SEE	0.318	0.272	0.218	0.098	0.100	0.282
F_{ratio}	42.351	48.299	83.155	340.286	326.846	55.660
r^2_{pred}	0.800	0.655	0.548	0.741	0.841	0.690
Component	4	5	4	6	6	6

[a]Statistical parameters have their original meanings. CF: column filtering

Table 3. Model progressive scrambling for CoMFA, CoMFA-RF and CoMSIA models based on docking alignment

Model	q^2	cSDEP	$dq^{2'}/dr^2\,yy'$
CoMFA	0.574	0.603	0.806
CoMFA-RF	0.581	0.598	1.033
CoMSIA	0.462	0.755	0.772

CoMFA and CoMSIA Results. The results of 3D-QSAR studies are summarized in Tables 2 and 3. PLS analysis of the docking alignment of the compounds in training set showed CoMFA-region focusing (CoMFA-RF) QSAR model (grid spacing = 1) with a good q^2 value of 0.756 (6 components) that is much better than common CoMFA. Also it can be seen that when the fields were focused, the CoMFA models improve in both methods of alignment and produce higher q^2 value. The optimal number of components evaluated by selecting the highest q^2 value corresponds to lowest S_{press} value. The non cross-validated PLS analysis results high r^2 value of 0.988, F_{value} of 326.846 and a low standard error of estimation (SEE) of 0.100. The outlier status of compound **5** in all 3D-QSAR models indicates its structural strangeness as there are only 3 compounds which have a methylene between phenyl and carbonyl groups and because of small category of these structures, this compound cannot be well predicted and thus identified as outlier and removed from the training set. Figure 5(a) shows the relationship between the experimental and predicted pIC_{50}.

The CoMSIA analysis was done using both methods of alignment at a grid spacing 2 Å, and the effect of column filtering was checked with the combination of five fields. The CoMSIA method defines hydrophobic and hydrogen bond donor and acceptor descriptors in addition to the steric and electrostatic fields in CoMFA. The combination of fields was systematically changed to select the optimal results.

In the first approach which the conformers were aligned to the template molecule in SYBYL program, by using the combination of three fields (steric, hydrophobic and hydrogen bond acceptor), q^2 of 0.617 was obtained with 4 component at a column filtering of 2.6 kcal/mol. The non cross-validated analysis results showed r^2 of 0.899, F = 83.155 and SEE = 0.218.

Also, CoMSIA 3D-QSAR study was performed on the compounds in the docking alignment method. In this method, all molecules were minimized inside the active site of tubulin and then docked by GOLD software in Discovery Studio program and then fed to SYBYL program. CoMSIA PLS analysis determined q^2 value of 0.673 with 6 PLS components by using the combination of four fields (steric, electrostatic, hydrophobic and hydrogen bond acceptor). The q^2 values of each independent field of steric, electrostatic, hydrophobic, hydrogen bond donor and hydrogen bond acceptor are 0.684, 0.550, 0.493, 0.022 and 0.333 respectively. The contribution of these four fields has significant effect on constructed model. Figure 5(b) shows the relationship between the experimental and predicted pIC50. The values of experimental and predicted activities of CoMFA and CoMSIA models are depicted in Table 4.

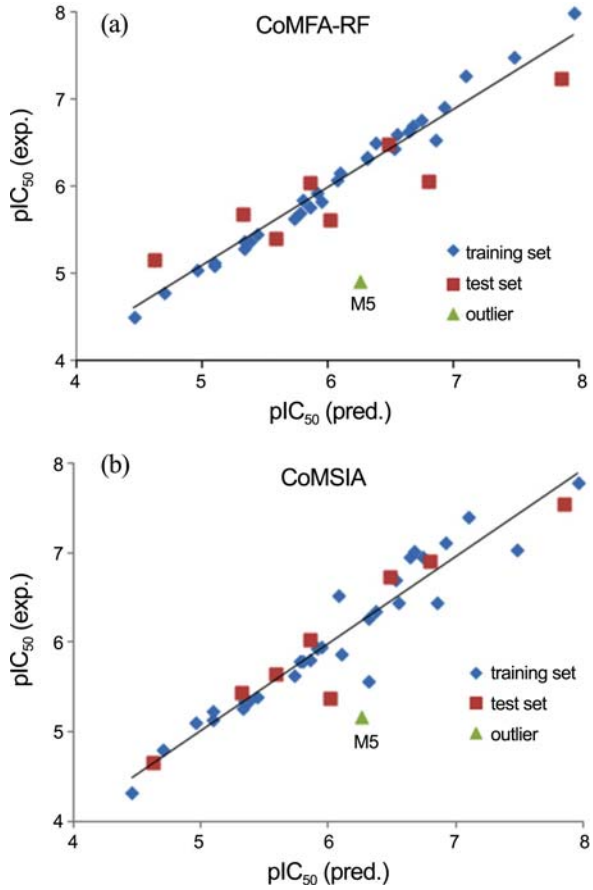

Figure 5. Observed against predicted activities for the training and test sets of compounds by docking alignment based on CoMFA-RF (a) and CoMSIA (b) models.

Validation of the 3D-QSAR Models. The external set of 8 compounds was used to confirm predictive ability of the models. The predictive correlation coefficient (r^2_{pred}) from CoMFA-RF and CoMSIA models in the rigid alignment method was found to be 0.655 and 0.548, and by using docking conformer, r^2_{pred} of 0.841 and 0.690 was achieved, respectively, which show models have acceptable predictability. It can be observed that by using docking conformer, the predictability of CoMFA and CoMSIA models increase greatly. To evaluate the statistical confidence limits of the derived models, bootstrapping[36] analysis was carried out with 100 runs. Bootstrapping includes the generation of many new datasets from the original dataset after randomly choosing samples from that. A r^2_{bs} (average correlation coefficient for bootstrapping) of 0.994 ± 0.003 and a SEE_{bs} (average standard error of estimate for bootstrapping) of 0.076 ± 0.052 for CoMFA-RF model in the docking alignment method, and r^2_{bs} of 0.973 ± 0.010, and a SEE_{bs} of 0.162 ± 0.103 for CoMSIA model generated by docking conformer, suggested a good internal consistency and the absence of systematic errors of the models. To evaluate the sensitivity of the optimized CoMFA-RF and CoMSIA models to chance correlations, the leave-one-out (LOO), leave 10-out cross-validation and progressive scrambling analyses were

Table 4. The experimental pIC50 values, predicted pIC50 values and the residuals of the training and test set compounds based on docking alignment

Compound No.	Experimental	CoMFA-RF		CoMSIA	
		Pred.	Res.	Pred.	Res.
1	7.4815	7.486	-0.0045	7.033	0.4485
2[a]	5.3178	5.679	-0.3612	5.443	-0.1252
3	6.8539	6.539	0.3149	6.438	0.4159
4	5.8601	5.758	0.1021	5.809	0.0511
5	6.2596	4.91	1.3496	5.173	1.0866
6	7.0969	7.263	-0.1661	7.396	-0.2991
7	5.3344	5.375	-0.0406	5.264	0.0704
8	5.9508	5.837	0.1138	5.946	0.0048
9[a]	4.6198	5.163	-0.5432	4.664	-0.0442
10	4.6989	4.787	-0.0881	4.797	-0.0981
11	5.9172	5.934	-0.0168	5.927	-0.0098
12	6.3098	6.324	-0.0142	5.566	0.7438
13[a]	6.7959	6.056	0.7399	6.906	-0.1101
14	6.6383	6.63	0.0083	6.958	-0.3197
15[a]	7.8539	7.236	0.6179	7.552	0.3019
16	7.9586	7.99	-0.0314	7.78	0.1786
17	6.3098	6.336	-0.0262	6.269	0.0408
18	6.9208	6.913	0.0078	7.11	-0.1892
19[a]	6.4815	6.481	0.0005	6.732	-0.2505
20	5.7305	5.626	0.1045	5.636	0.0945
21	6.6778	6.687	-0.0092	7.024	-0.3462
22	6.0757	6.068	0.0077	6.518	-0.4423
23	4.9586	5.044	-0.0854	5.106	-0.1474
24	5.0969	5.132	-0.0351	5.131	-0.0341
25	5.3372	5.282	0.0552	5.349	-0.0118
26[a]	6.0132	5.61	0.4032	5.372	0.6412
27	5.4413	5.46	-0.0187	5.386	0.0553
28	6.3767	6.503	-0.1263	6.349	0.0277
29	5.0953	5.099	-0.0037	5.225	-0.1297
30	6.5229	6.427	0.0959	6.694	-0.1711
31[a]	5.8539	6.047	-0.1931	6.035	-0.1811
32	4.4559	4.509	-0.0531	4.33	0.1259
33	5.7825	5.701	0.0815	5.786	-0.0035
34	6.5528	6.603	-0.0502	6.439	0.1138
35[a]	5.585	5.399	0.186	5.643	-0.058
36	6.7447	6.767	-0.0223	6.961	-0.2163
37	6.0969	6.154	-0.0571	5.863	0.2339
38	5.3767	5.37	0.0067	5.336	0.0407
39	5.8013	5.85	-0.0487	5.792	0.0093

[a]Prediction set

performed.[37] The q^2 values of leave 10-out for CoMFA-RF and CoMSIA models without using docking conformer were 0.554 and 0.624 and with using docking conformer were 0.737 and 0.659 respectively. In the progressive scrambling approach, small random perturbations are introduced into a data set and the statistical results. The perturbation prediction (q^2), the calculated cross-validated standard error of prediction (cSDEP) as the function of the correlation coefficient between the true values (y) of the dependent variables and the perturbed values (y') of the dependent variables, and the slope of q^2 (cross validated correlation coefficient) with respect correlation of the original dependent variables against the perturbed dependent variables ($d_q^{2'}/dr^2_{yy'}$), for CoMFA-RF and CoMSIA models are summarized in Table 3.

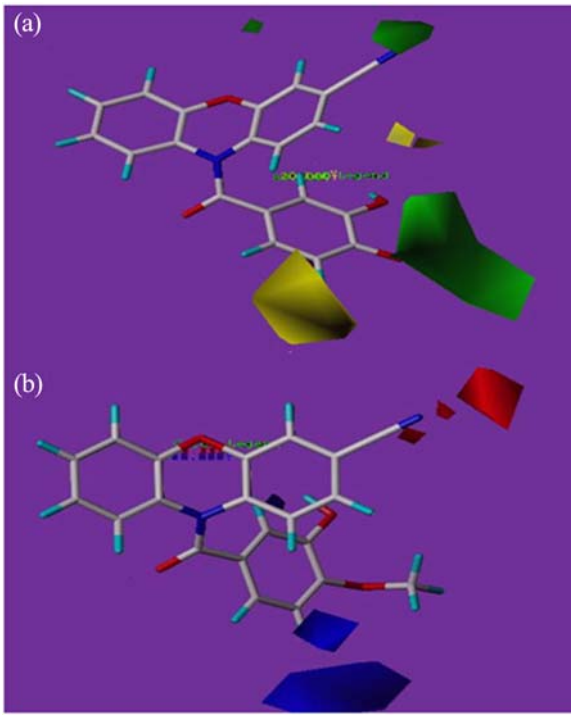

Figure 6. CoMFA contour map displaying steric (a) and electrostatic (b) in combination with compound **16** based on docking alignment method. Green contours show contribution for sterically favorable interactions with the receptor and yellow contours show sterically unfavorable regions, while blue and red contours show electropositive and electronegative charge favorable regions, respectively.

CoMFA Contour Maps Analysis. The CoMFA steric and electrostatic fields from the final best non cross-validated analysis were plotted as 3D colored contour maps. The contour maps of CoMFA denote the region in the space where the aligned molecules would favorably or unfavorably interact with the receptor. The contour maps using region focusing are of better quality because the region focusing resulted in a sort of image enhancement. In the CoMFA steric contour maps, green contours show contribution for sterically favorable interactions with the receptor and yellow contours show sterically unfavorable regions, these contours represent 80% and 20% contributions, respectively. Similarly blue contours show the regions that are electropositive charge favorable and red contours show electronegative charge favorable regions that their contributions in the CoMFA electrostatic field represent 80% and 20% respectively. Greater values of bio-activity are correlated with more bulk near green, less bulk near yellow more positive charge near blue and more negative charge near red.

The contours for CoMFA-RF steric and electrostatic fields are displayed in Figure 6. In this case, compound **16** was used as a reference to show the contour maps of the CoMFA model. The large yellow region around R_7 substituent, suggest that a less sterically bulky group is favorable and increase

the activity such that the antiproliferative activity of compounds **3** and **6** with hydrogen atom at that region is higher than compound **9** with methoxy group. A yellow region near R_2 substituent indicates that bulky groups in this region will decrease the activity. A large region of green contour near R_6 suggest that more potent analogs may be obtained by introducing bulky substituents such as methoxy group to this region. In CoMFA-RF electrostatic contour maps, there are red contours near R_1 substituent (Figure 6(b)) that shows electronegative groups such as CN in this situation increase the antiproliferative activity, in such a way, compounds **15** and **16** are the most active compounds in the set. There are blue regions near R_7 witch explain electropositive substituents would increase the activity. It can be demonstrated by comparing the structures and activities of compounds **9** (R_7 = OCH_3, pIC_{50} = 4.6198) with **3** (R_7 = H, pIC_{50} = 6.8539) and compound **35** (R_7 = OCH_3, pIC_{50} = 5.5850) with **34** (R_7 = H, pIC_{50} = 6.5528) and **36** (R_7 = H, pIC_{50} = 6.7447).

CoMSIA Contour Map Analysis. The advantage of CoMSIA contour maps over CoMFA is that they are easier to interpret. Compound **16** was used as a reference to show the contour maps of the CoMSIA model. The steric field distribution of CoMSIA model is shown in Figure 7(a). By comparison of Figure 7(a) with Figure 6(a), it can be seen that CoMSIA steric contour maps is similar to CoMFA steric contour maps. In the CoMSIA electrostatic contour maps, there is a big red contour covers x substituent. This indicates

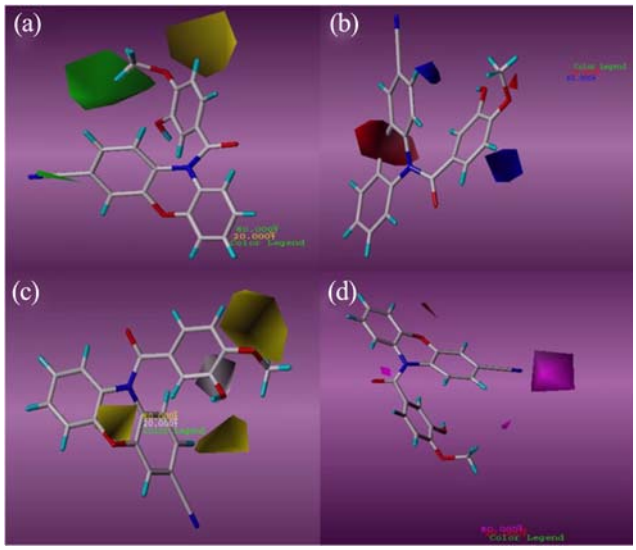

Figure 7. CoMSIA contour map displaying steric (a), electrostatic (b), hydrophobic (c), hydrogen bond acceptor (d) in combination with compound **16** based on docking alignment method. Based on steric contour map, Green and yellow contours show contribution for sterically favorable and unfavorable interactions with the receptor, respectively, while blue and red contours in electrostatic fields show electropositive and electronegative charge favorable regions respectively. In the hydrophobic contour map, yellow and white regions indicate the areas where hydrophobic and hydrophilic properties are preferred, respectively, while in hydrogen bond acceptor field, magenta contours show regions where hydrogen bond acceptor groups are favored and red contours indicate regions where hydrogen bond acceptor groups are unfavorable.

that electronegative groups in this position increase antiproliferative activity, Figure 7(b). This is a sensible reason why compound **1** (x = O, pIC_{50} = 7.4815) has higher activity than compounds **19**, **28** and **34** (x = S, pIC_{50} = 6.4815; x = SO, pIC_{50} = 6.3767 and x = SO2, pIC_{50} = 6.5528). Two blue contours near R_2 and R_7 shows that electropositive substituents would increase the activity. That's why compound **28** (R_2 = H, R_7 = H, pIC_{50} = 6.3767) has higher activity than compounds **31** and **32** (R_2 = Cl, R_7 = H, pIC_{50} = 5.8539 and R_2 = Cl, R_7 = OCH_3, pIC_{50} = 4.4559).

In the hydrophobic contour map of CoMSIA, Figure 7(c), yellow and white regions indicate the areas where hydrophobic and hydrophilic properties are preferred, respectively. A white contour is found near the R_5 substituent which explains the necessity of the hydrophilic group to increase the activity. This can explain the order of activities in these compounds: 6 > 3 > 9 that is based on descending of the hydrophilic property. According to docking results in this area there is an interaction with hydrophilic residues of receptor, *i.e.* the NH group of Leu255 and the C=O group of Lys254 (β chain) that confirm CoMSIA's hydrophobic contour. Three yellow contours near the x group, R_2 and R_6 indicate that hydrophobic groups in these areas are preferred for antiproliferative activity. It can be demonstrated by comparing the structures and activities of compound **19** (R_2 = H, pIC_{50} = 6.4815) with **22** (R_2 = Cl, pIC_{50} = 6.0757), compound **3** (R_6 = OCH_3, pIC_{50} = 6.8539) with **10** (R_6 = Cl, pIC_{50} = 4.6989) and compound **1** (x = O, pIC_{50} = 7.4815) with **34** (x = SO_2, pIC_{50} = 6.5528).

Based on hydrogen bond acceptor field in Figure 7(d), magenta contours show regions where hydrogen bond acceptor groups are favored and red contours indicate regions where hydrogen bond acceptor groups are unfavorable for increasing activity. There is one magenta contour near R_1 substituent that suggest hydrogen bond acceptor in this region is favored. Complementary of this magenta contour in the receptor, is hydrogen bond donor group (Cys241). This is the reason why compounds **15** and **16** with CN group at this position are the most active compounds in the set. Also presence of electrostatic red contour at this region confirms the magenta contour.

Conclusion

The analysis of 39 tubulin polymerization inhibitors by molecular docking and 3D-QSAR studies provides a good predictive model for the design of new series of antitumor drugs. In this study, 3D-QSAR models were generated by two different methods, by using docked ligands as bioactive conformers and without docked ligands. The comparison of these models demonstrates that CoMFA and CoMSIA models based on docking alignment method have more reliable contour maps. The CoMFA and CoMSIA analysis have provided distinguishing key structural features affecting activity of these inhibitors. We identified and confirmed the residues that play key role in the hydrogen bond donors, hydrogen bond acceptors, hydrophobic, steric and electrostatic inter-

actions. The great statistical parameters and suitable predictive ability of the generated models may provide a useful guideline to design and predict the activity of novel compounds with enhanced inhibitory activities and can help to rational design of novel anticancer drugs.

References

1. Checchi, P. M.; Nettles, J. H.; Zhou, J.; Snyder, J. P.; Joshi, H. C. *Trends Pharmacol. Sci.* **2003**, *24*, 361.
2. Nogales, E. *Annu. Rev. Biochem.* **2000**, *69*, 277.
3. Jordan, M. A.; Wilson, L. *Nat. Rev. Cancer* **2004**, *4*, 253.
4. Valiron, O.; Caudron, N.; Job, D. *Cell Mol. Life Sci.* **2001**, *58*, 2069.
5. Jordan, A.; Hadfield, J. A.; Lawrence, N. J.; McGown, A. T. *Med. Res. Rev.* **1998**, *18*, 259.
6. Seibel, N. L.; Reaman, G. H. *Invest. New Drugs* **1996**, *14*, 49.
7. Schiff, P. B.; Horwitz, S. B. *Proc. Natl. Acad. Sci. U.S.A.* **1980**, *77*, 1561.
8. Pellegrini, F.; Budman, D. R. *Cancer Invest.* **2005**, *23*, 264.
9. Hearn, B. R.; Shaw, S. J.; Myles, D. C. *Compr. Med. Chem. II* **2007**, *7*, 81.
10. Li, Q.; Sham, H. L. *Expert Opin. Ther. Patents* **2002**, *12*, 1663.
11. Hadfield, J. A.; Ducki, S.; Hirst, N.; McGown, A. T. *Prog. Cell Cycle Res.* **2003**, *5*, 309.
12. Ghasemi, J. B.; Meftahi, N. *J. Enzyme Inhib. Med. Chem.* **2013**, *28*, 320.
13. Lill, M. A. *Drug Discov. Today* **2007**, *12*, 1013.
14. Yang, G. F.; Huang, X. *Curr. Pharm. Des.* **2006**, *12*, 4601.
15. Pirhadi, S.; Ghasemi, J. B. *Eur. J. Med. Chem.* **2010**, *45*, 4897.
16. Gayathri, P.; Pande, V.; Sivakumar, R.; Gupta, S. P. *Bioorg. Med. Chem.* **2001**, *9*, 3059.
17. Cramer, R. D.; Patterson, D. E.; Bunce, J. D. *J. Am. Chem. Soc.* **1988**, *110*, 5959.
18. Klebe, G.; Abraham, U.; Mietzner, T. *J. Med. Chem.* **1994**, *37*, 4130.
19. Ghasemi, J. B.; Pirhadi, S.; Ayati, M. *Bull. Korean Chem. Soc.* **2011**, *32*, 645.
20. Sirois, S.; Wei, D. Q.; Du, Q. S.; Chou, K. C. *J. Chem. Inf. Comput. Sci.* **2004**, *44*. 1111.
21. Liao, Q. H.; Gao, Q. Z.; Wei, J.; Chou, K. C. *Med. Chem.* **2011**, *7*, 24.
22. Liu, X. Y.; Wang, R. L.; Xu, W. R.; Tang, L. D.; Wang, S. Q.; Chou, K. C. *Protein. Peptide. Lett.* **2011**, *18*, 1021.
23. Chou, K. C. *Curr. Med. Chem.* **2004**, *11*, 2105.
24. Zhao, T. T.; Lu, X.; Yang, X. H.; Wang, L. M.; Li, X.; Wang, Z. C.; Gong, H. B.; Zhu, H. L. *Bioorg. Med. Chem.* **2012**, *20*, 3233.
25. Liao, S. Y.; Chen, J. C.; Miao, T. F.; Shen, Y.; Zheng, K. C. *J. Enzyme Inhib. Med. Chem.* **2010**, *25*, 421.
26. Liao, S. Y.; Qian, L.; Miao, T. F.; Lu, H. L.; Zheng, K. C. *Eur. J. Med. Chem.* **2009**, *44*, 2822.
27. Prinz, H.; Chamasmani, B.; Vogel, K.; Bohm, K. J.; Aicher, B.; Gerlach, M.; Gunther, E. G.; Amon, P.; Ivanov, I.; Muller, K. *J. Med. Chem.* **2011**, *54*, 4247.
28. Momany, F. A.; Rone, R. J. *J. Comput. Chem.* **1992**, *13*, 888.
29. Discovery Studio. Accelrys Software Inc, San Diego, CA, 2009.
30. Politi, A.; Durdagi, S.; Moutevelis-Minakakis, P.; Kokotos, G.; Mavromoustakos, T. *J. Mol. Graph. Model* **2010**, *29*, 425.
31. http://www.ccdc.cam.ac.uk/support/documentation/gold/3_1/gold31.pdf.
32. Tripos, QSARTM Manual, SYBYL, version 7.3, 2006, St. Louis, 2006.
33. Baroni, M.; Costantino, G.; Cruciani, G.; Riganelli, D.; Valigi, R.; Clementi, S. *Quant. Struct.-Act. Relat.* **1993**, *12*, 9.
34. Cho, S. J.; Tropsha, A. *J. Med. Chem.* **1995**, *38*, 1060.
35. Wang, R.; Gao, Y.; Liu, L.; Lai, L. *J. Mol. Model* **1998**, *4*, 276.
36. Cramer, R. D.; Patterson, D. E.; Bunce, J. D. *J. Am. Chem. Soc.* **1988**, *110*, 5959.
37. Clark, R.; Fox, P. *J. Comput. Aided Mol. Des.* **2004**, *18*, 563.